

## Aircraft measurements and numerical simulations of mountain waves over the central Alps: A pre-MAP test case

By JAMES D. DOYLE<sup>1\*</sup>, HANS VOLKERT<sup>2</sup>, ANDREAS DÖRNBRACK<sup>2</sup>, KLAUS P. HOINKA<sup>2</sup> and  
TIMOTHY F. HOGAN<sup>1</sup>

<sup>1</sup>*Naval Research Laboratory, Monterey, USA*

<sup>2</sup>*Institut für Physik der Atmosphäre, Germany*

(Received 26 July 2001; revised 10 April 2002)

### SUMMARY

In preparation for the field phase of the Mesoscale Alpine Project (MAP), *in situ* research-aircraft observations from the DLR Falcon, and three-dimensional high-resolution numerical simulations are used to investigate mountain waves generated during a south föhn event on 10 October 1987. The model simulation qualitatively compares favourably with the aircraft observations in terms of identifying the horizontal and vertical locations of maximum gravity-wave amplitude and rapid decay of wave amplitudes in the lower stratosphere. However, even with reasonably specified large-scale conditions, the vertical velocity and temperature perturbations are not in quantitative agreement with the aircraft measurements. The results highlight some deficiencies that still exist in our predictive capability to simulate gravity-wave generation and propagation explicitly over three-dimensional topography for non-steady conditions. The complexity of the gravity-wave response points toward the necessity of a straightforward aircraft observing strategy that features linear flight segments oriented along the cross-mountain wind direction, a rapid repetition of these segments in order to assess the significance of transients, and a combination of *in situ* measurements with remote-sensing data (e.g. from lidar systems and dropsondes), an approach that was successfully applied during the MAP.

KEYWORDS: Föhn Gravity waves Mesoscale Alpine Project Numerical modelling

### 1. INTRODUCTION

The Mesoscale Alpine Project (MAP) is a coordinated international effort to examine moist and dry processes associated with three-dimensional complex topographic flows including gravity-wave generation and breaking, which culminated in a two-month field phase during the autumn of 1999 (Bougeault *et al.* 2001). During the field phase of the MAP, high-resolution numerical simulations were used as guidance for aircraft missions designed to observe mountain-wave breaking. In preparation for the MAP field phase, a collaborative effort was established to evaluate the capability of high-resolution numerical models to predict the location of mountain-wave excitation, amplification, and turbulent breakdown in a series of experiments involving airflow over topography. The first test, a multi-model intercomparison of a series of two-dimensional, high-resolution numerical simulations, demonstrated that models are capable of simulating breaking in comparable horizontal locations and vertical layers (Doyle *et al.* 2000). In the present study, which served as a second, more challenging, test, simulations from a non-hydrostatic numerical modelling system are compared with aircraft observations from a well documented gravity-wave case over the Alps (10 October 1987) in order to evaluate the capability of current numerical models to predict gravity-wave generation and propagation adequately over complex topography with time-dependent flow. In this note, we document the results from the most detailed study involving measurements and numerical simulations performed during the planning phase of the MAP. The specific focus of this study is on modest amplitude topographically-forced gravity waves that were anticipated before the MAP to be common over the central Alps and were frequently encountered during the field phase (Bougeault *et al.* 2001; Smith *et al.* 2002).

Internal gravity waves are generated as stably stratified airflows over a topographic obstacle. Under some circumstances, mountain waves may propagate upward into the stratosphere, amplify due to the decrease of density and undergo turbulent breakdown. Mountain-wave breaking is thought to have an important influence on the atmosphere for reasons that include: potential-vorticity generation due to non-conservative processes (Schär and Smith 1993), downslope windstorms (Clark and Peltier 1977), clear-air turbulence (Lilly 1978), vertical mixing within breaking layers (Dörnbrack and Dürbeck 1998), and the collective effect of wave breakdown on the atmospheric general circulation (Bretherton 1969). When a low-level wave guide is present due to the variation with height of the static stability and cross-mountain

\* Corresponding author: Naval Research Laboratory, Marine Meteorology Division, 7 Grace Hopper Avenue, Monterey, CA 93943-5502, USA. e-mail: doyle@nrlmry.navy.mil

air stream (e.g. Durran 1990), vertically propagating gravity waves may be ducted leading to resonant lee-waves generation. Real-time mesoscale models during the MAP often failed to predict trapped lee waves adequately (Bougeault *et al.* 2001).

There have been numerous studies that have applied numerical models to investigate the dynamics of topographically-forced gravity waves (e.g. Wurtele *et al.* 1996). Several investigations are available of gravity waves forced by orography such as the Rocky Mountains (Ralph *et al.* 1997; Clark *et al.* 2000) and the Pyrenees during the Pyrenees Experiment (PYREX) (Satomura and Bougeault 1994; Broad 1996). However, one important difference between the Rocky Mountains as well as the Pyrenees and the Alps is that the latter orographic barrier contains a greater variety of mesoscale to smaller-scale variations. In the Alps, numerous high ridges with steep valleys are oriented in a variety of geographical directions and can force local circulations, which may influence the larger-scale cross-mountain flow significantly and ultimately the gravity-wave properties. One of the objectives of the MAP is to improve our understanding of three-dimensional gravity-wave propagation and breaking associated with flow over complex three-dimensional orography, such as the Alps. Before the MAP there have been relatively few investigations of gravity waves forced by complex three-dimensional topography, and even fewer which used available *in situ* aircraft data. The general aim of this study is to assess the capability of a state-of-the-science high-resolution numerical model to simulate gravity waves over three-dimensional irregular topography and, at the same time, to illustrate some current limitations for reliable predictions of gravity waves.

## 2. MODEL DESCRIPTION AND SYNOPTIC-SCALE OVERVIEW

The atmospheric portion of the Coupled Ocean/Atmosphere Mesoscale Prediction System (COAMPS) (Hodur 1997) is applied in this study. The numerical model is a finite-difference approximation to the fully compressible, non-hydrostatic equations and uses a terrain-following vertical coordinate transformation. A suite of parametrizations is used to represent physical processes, such as those due to radiation, convection, clouds and microphysics, and boundary-layer turbulence. The COAMPS simulations make use of five nested grids with horizontal grid increments of 45, 15, 5, 1.7, and 0.56 km with 55 vertical levels. A radiation upper boundary condition is used to minimize the reflection of vertically propagating gravity waves. The lateral boundary conditions are specified using the Navy Operational Global Atmospheric Prediction System (NOGAPS) analyses. The COAMPS model was initialized at 0000 UTC 10 October and integrated to 1700 UTC 10 October.

Föhn conditions that were characterized by strong synoptic-scale southerly flow were established over the central Alps on 10 October 1987. This event is noteworthy because of the strength, which resulted in localized wind damage in the central Alps, and the unique set of aircraft measurements that were performed using the DLR\* Falcon research aircraft to document the gravity-wave characteristics. The Milan sounding for 1200 UTC 10 October 1987 (Fig. 1) exhibits the conditions that are typical for a south föhn, with easterly flow below crest height (about 3 km) indicative of flow blocking, the presence of strong southerly flow of  $15 \text{ m s}^{-1}$  at crest height and above, and a weak inversion near 7 km above sea level (asl). The southerly flow extends throughout the troposphere with little directional shear above 4 km (Fig. 1), which is conducive for deep vertical wave propagation in an atmosphere with vertically uniform static stability and winds (e.g. Shutts 1998).

The characteristics of orographically generated gravity waves in the linear regime are primarily governed by mountain shape, size, and the Scorer parameter,

$$l^2 = \frac{N^2}{U^2} - \frac{1}{U} \frac{\partial^2 U}{\partial z^2}, \quad (1)$$

where  $U(z)$  is the cross-mountain wind speed,  $N(z)$  is the Brunt-Väisällä frequency, and  $z$  is the vertical coordinate. Scorer (1949) found that if  $l^2$  decreases rapidly with height, resonant lee waves can develop in the lower atmosphere. The Scorer parameter profile upstream of the Alps, computed based on the Milan sounding and shown in Fig. 1(c), indicates a rapid decrease of  $l^2$  with height in the lowest 3 km of the atmosphere. The decrease of  $l^2$  with height is primarily a result of the vertical shear of the cross-mountain wind component in the topographically blocked layer below approximately 2.5 km. Above this blocked layer, the profile indicates that  $l^2$  generally decreases in the 3–6 km layer, which is suggestive that the mean state is capable of supporting trapped modes. However, gravity waves longer than the critical horizontal wavelength,  $\lambda_c = 2\pi/l$ , can propagate vertically through the wave duct. In this case  $\lambda_c$  is approximately 5–10 km in the lower troposphere above the blocked layer. Clearly, in this situation linear theory must be applied with some caution, particularly considering the steep three-dimensional topography

\* Deutsches Zentrum für Luft- und Raumfahrt.

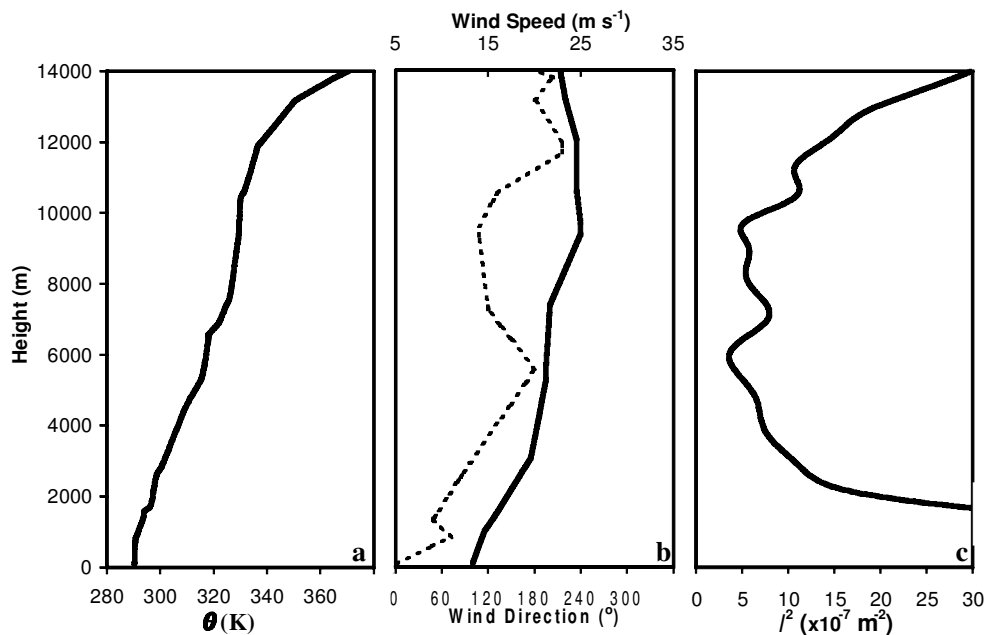


Figure 1. Profiles of (a) potential temperature, (b) wind direction (full line) and speed (dashed line) and (c) Scorer parameter from the radiosonde at Milan valid at 1200 UTC 10 October 1987.

of the central Alps. Visible satellite imagery for 10 October indicates the presence of scattered clouds over northern Italy and numerous north-west to south-east oriented banded structures or lenticularis clouds, often associated with gravity-wave or lee-wave activity, located to the north of the Alpine crest.

### 3. RESULTS

#### (a) Aircraft observations

Two research-aircraft missions were conducted on 10 October 1987 using the DLR Falcon. The first set of measurements was taken in the morning from 0910–1210 UTC and the second set in the afternoon from 1335–1637 UTC. The flight track, projected over the Alpine terrain and shown in Fig. 2, consisted of a series of four trans-Alpine flight segments along A–B–C–D (Munich to Vicenza) and two northern legs along E–F and G–H. The track traversed a massif near  $46.75^{\circ}\text{N}$  (Sarntaler Alpen), the Brenner Pass near  $47^{\circ}\text{N}, 11.5^{\circ}\text{W}$ , which is the topographic minimum along the Alpine crest, the steep western flanks of the Wipp valley, the deep Inn valley, and the Karwendel ranges to the north. The flight segments were executed at six vertical levels ranging from 1.5 km to 10.8 km asl. The complex flight track was unavoidable in this case due to air traffic control constraints.

Isentropic analyses, based on the aircraft measurements for the flights at 0910–1210 UTC and 1335–1637 UTC, are shown in Figs. 3(a) and (b), respectively. Moderate-amplitude gravity waves are present for both the morning and afternoon flights. The largest-amplitude gravity wave is apparent near 6 km above the Alpine crest during the afternoon only, indicative of the non-steady character of the flow. The three dimensionality of the topography makes interpretation of the two-dimensional analysis difficult (e.g. Hoinka and Clark 1991). For example, the aircraft may have encountered horizontally propagating gravity waves that were forced by the topographic peaks located near but not along the flight track. It is noteworthy that the potential-temperature signatures of the gravity waves are not particularly well correlated in the vertical, which underscores the time-dependent nature of the flow in this case and three dimensionality of the underlying terrain. Additionally, some of the lack of vertical correlation in the isentropic analysis may result from the time lag between flight segments at the various altitudes (see Fig. 8).

Flight-level vertical-velocity measurements from the Falcon for six different altitudes, valid between 1335–1637 UTC, are shown in Fig. 4. The largest-amplitude waves, with a maximum vertical velocity of  $5.5 \text{ m s}^{-1}$ , are located over the slopes south of the Inn Valley along segment B–C and positioned vertically

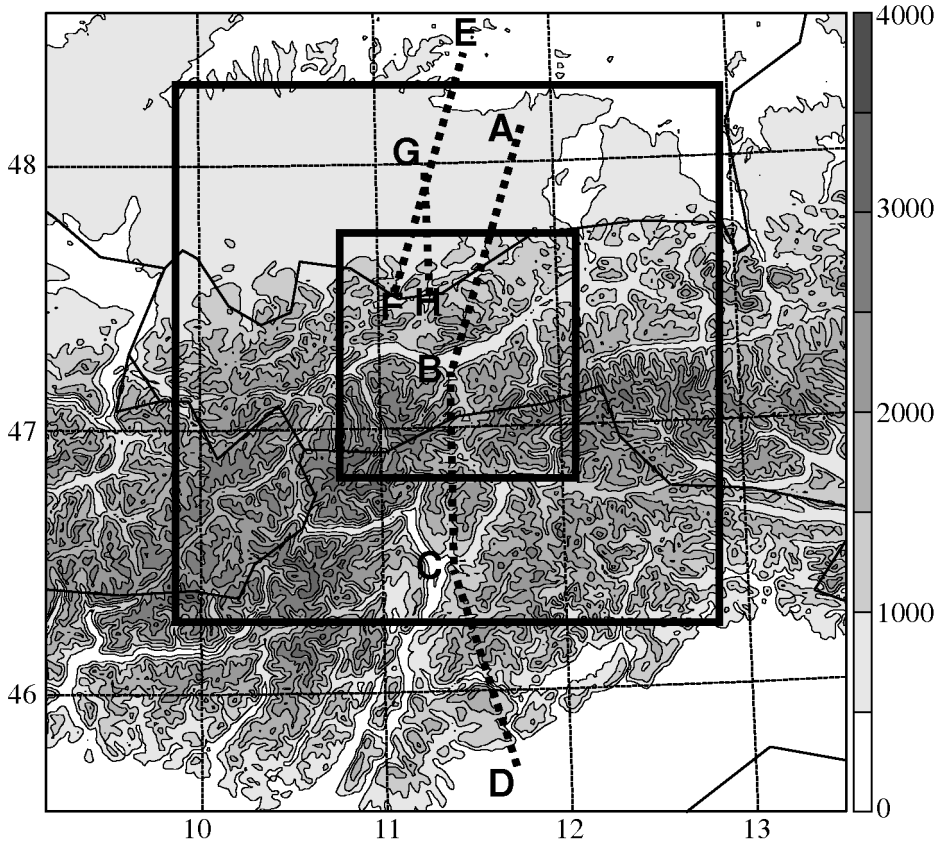


Figure 2. The topography of the central Alps (m) and model nested domain locations for the fourth ( $\Delta x = 1.7$  km) and fifth ( $\Delta x = 0.56$  km) grid meshes. The medium thickness full lines represent the political boundaries. Longitude ( $^{\circ}$ E) and latitude ( $^{\circ}$ N) are displayed every  $1^{\circ}$  and labelled along the abscissa and ordinate, respectively. The dashed lines represent flight segments and the letters A to H represent way points (see text).

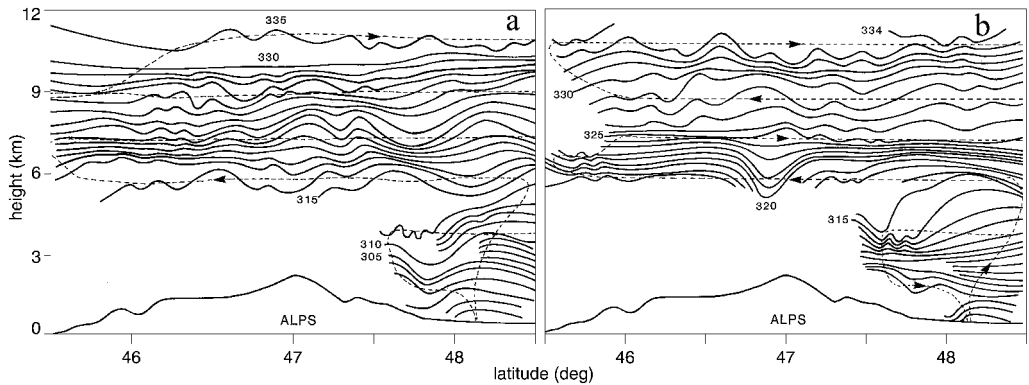


Figure 3. Manual isentropic analyses based on research aircraft flight-level data for (a) 0910–1210 UTC and (b) 1335–1637 UTC 10 October 1987. The isentropes are shown every 1 K and the flight track is dashed. The smoothed Alpine topography is plotted along the abscissa. (Adapted from Hoinka 1990.)

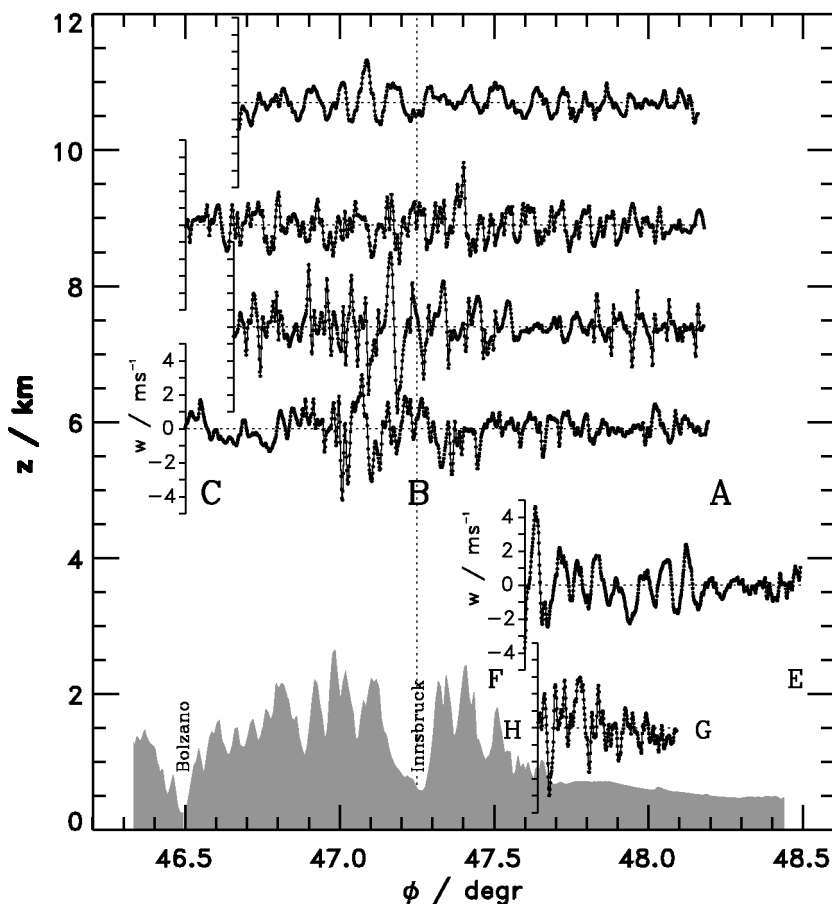


Figure 4. Vertical-velocity measurements ( $\text{m s}^{-1}$ ) at six different altitudes for the flight paths shown in Fig. 2 based on the afternoon flight (1335–1637 UTC 10 October 1987). Small dots representing measurements every second are joined by a thin line. The underlying orography is extracted from a digital elevation model with 1 km resolution. Capital letters designate the way points given in Fig. 2.

at 7.4 km. Vertical velocities are greater than  $4 \text{ m s}^{-1}$  in the lee of the crest to the north of Innsbruck along the segment F–E near 3 km. The mountain-wave amplitudes are significantly reduced at the higher-altitude legs. The regions above the southern portion of the Inn Valley and in the lee north of the Alpine crest contain the most significant temperature perturbations (not displayed). The vertical velocity and temperature perturbations are generally not vertically coherent, in agreement with the isentropic analyses (Fig. 3). The potential-temperature analysis (Fig. 3) and vertical-velocity observations (Fig. 4) suggest the presence of both trapped and vertically propagating waves rather than only stationary trapped lee waves, which would exhibit a more coherent vertical and temporal structure (e.g. Shutts and Broad 1993; Broad 1996). Further details concerning the 10 October 1987 föhn case, as well as analyses and simulations using the tools available a decade ago, are contained in Hoinka (1990).

#### (b) Model simulation

The model simulations of the 10 October 1987 föhn event suggest that the strong southerly flow in the lower troposphere that was forced over the three-dimensional orography of the central Alps, resulted in generation of a complex pattern of gravity waves. The simulated vertical velocity for 1100 UTC and 1400 UTC at 7400 m for the inner-grid mesh ( $\Delta x = 0.56 \text{ km}$ ), shown in Fig. 5, illustrates the complex gravity-wave response. The observed maximum gravity-wave amplitude is located at this level (Fig. 4) for the afternoon flight. The simulation at 1100 UTC (Fig. 5(a)), corresponding to the morning flight, indicates larger-amplitude waves and more of a tendency for lee waves to extend further downstream than is apparent

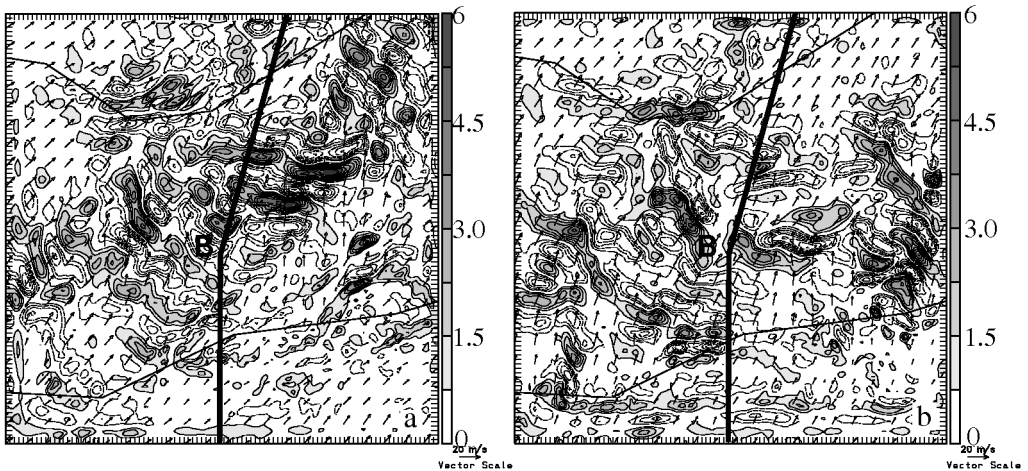


Figure 5. Model simulated vertical velocity and winds at the 7400 m level for (a) 1100 UTC and (b) 1400 UTC 10 October 1987. The upward vertical velocity contours greater than  $0.75 \text{ m s}^{-1}$  are shaded using the grey scale. The contour interval is  $0.75 \text{ m s}^{-1}$  with dashed contours indicating descent. The thick full line denotes the flight path (see Fig. 2). Superimposed are horizontal wind vectors at every 5th grid point in either direction (cf. tick marks at the perimeter).

in the simulation at 1400 UTC (Fig. 5(b)). These characteristics are also evident in the analyses of the aircraft potential-temperature measurements (Fig. 3). The simulated maximum vertical velocity for the 1100 UTC time is  $7.3 \text{ m s}^{-1}$  and is located in the lee of the highest topography in the central Alps, approximately 11 km to the east of the flight segment. The simulation at 1400 UTC indicates that a vertical velocity maximum of  $5.5 \text{ m s}^{-1}$  is located approximately 5 km to the west of the flight track near point B and is of similar magnitude to that of the observed maximum of  $5\text{--}6 \text{ m s}^{-1}$  measured at 7400 m at approximately 1445 UTC 10 October (Fig. 4). For both of the simulation times, the vertical velocity maximum is located to the north of the Inn Valley immediately downstream of the Alpine crest, similar to that observed. Noteworthy is the significant temporal variation in the vertical velocity pattern between morning and afternoon, which is also evident in the simulation at other heights. Resonant waves in the vertical velocity field are more apparent in the simulation at 1100 UTC than 1400 UTC, although a number of banded structures are evident at both times, in general agreement with the visible satellite imagery.

A vertical cross-section of simulated potential temperature and vertical velocity, along the flight path within the innermost domain (Fig. 2), is shown in Fig. 6 for 1400 UTC. At this time, the gravity waves appear to be vertically propagating and exhibit a characteristic upstream phase tilt (Smith 1979). The static stability upwind of the highest peaks and Brenner Pass is stronger in the lowest 5 km compared with the mid-troposphere, which is conducive for strong wave generation. The largest simulated vertical velocities are positioned above the slopes of the Inn Valley, co-located with low-level wave breaking as indicated by the local static stability minimum immediately upstream of point B associated with the steepening of isentropes.

The gravity waves on 10 October were quite transient, as suggested by the time series from 0900–1700 UTC of simulated vertical velocity at 7400 m constructed along the flight path (Fig. 2), shown in Fig. 7. The greatest-amplitude waves occur downstream of the Alpine crest and of point B. The wave amplitude at 7400 m is the largest before 1300 UTC. Additionally, the gravity waves appear to be more coherent with time before 1500 UTC, with the largest-amplitude waves exhibiting a tendency for weak upstream propagation.

In spite of the general qualitative agreement between the model-simulation results and aircraft observations, the predictive capability appears to be limited in this case with regard to the quantitative depiction of the mountain waves. Simulated and measured vertical velocity are shown in Fig. 8 for the 5800, 7400, and 10 800 m levels for the morning and afternoon flights. The model captures the approximate wavelength and amplitude of the waves as well as the general location along the flight track where the largest-amplitude waves were observed. Also, the model captures the general tendency for smaller-amplitude waves at the higher altitude (10 800 m) in comparison with the mid-tropospheric altitudes. However, clearly the model does not capture accurately the individual wave crests observed by the Falcon.

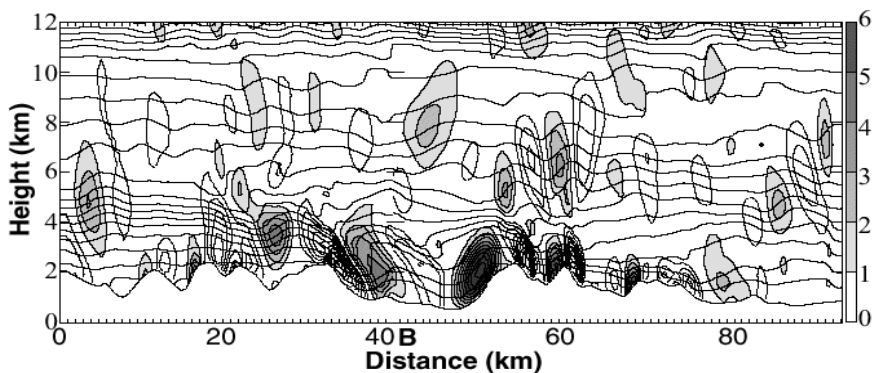


Figure 6. Model-simulated cross-section of vertical velocity and potential temperature for 1400 UTC 10 October 1987. The upward vertical velocity contours greater than  $1 \text{ m s}^{-1}$  are shaded using the grey scale. The vertical velocity contour interval is  $1 \text{ m s}^{-1}$  with dashed contours indicating descent. The isentropes correspond to the thick contours and are shown every  $2.5 \text{ K}$ . The section is located along the approximate flight track in Fig. 5 (south at the left side).

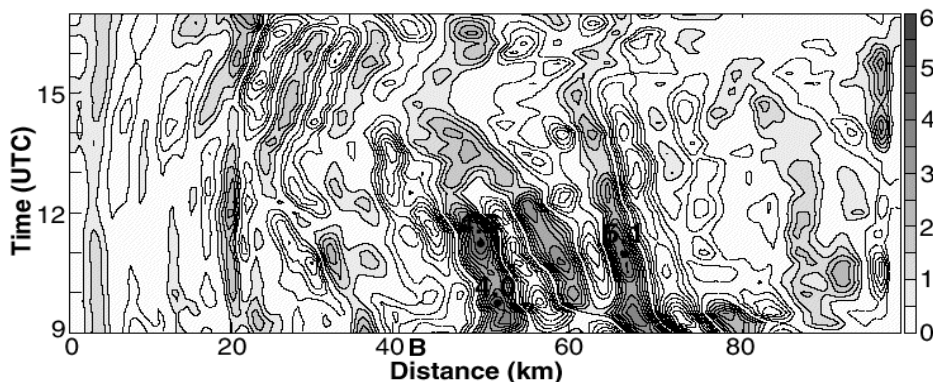


Figure 7. Time series of simulated vertical velocity for 0900–1700 UTC 10 October 1987 constructed along the flight path for the inner domain (Fig. 5; south at the left side) at  $7400 \text{ m}$ . The upward vertical velocity contours greater than  $0.5 \text{ m s}^{-1}$  are shaded using the grey scale. The vertical velocity contour interval is  $0.5 \text{ m s}^{-1}$  with dashed contours indicating descent.

#### 4. CONCLUSIONS

In this study, gravity-wave generation and propagation that occurred during a south föhn event on 10 October 1987 was examined. This gravity-wave event was selected as one of the pre-MAP test cases because of the expected occurrence of south föhn events during the MAP and the *in situ* measurements available to evaluate the model simulations. The model simulations from the COAMPS fine mesh ( $\Delta x = 0.56 \text{ km}$ ) compared favourably with the aircraft observations in terms of identifying the south edge of the Inn Valley as the location of maximum gravity-wave excitation. Additionally, the model successfully reproduced the rapid decay of wave amplitude between 9–11 km as observed by the aircraft. However, the specific locations of the model simulated vertical velocity and temperature perturbations do not agree particularly well with the aircraft observations. These experiments along with previously documented numerical simulations performed in preparation for the MAP (e.g. Doyle *et al.* 2000) have established the current capability of sophisticated non-hydrostatic modelling systems for the prediction of mountain wave

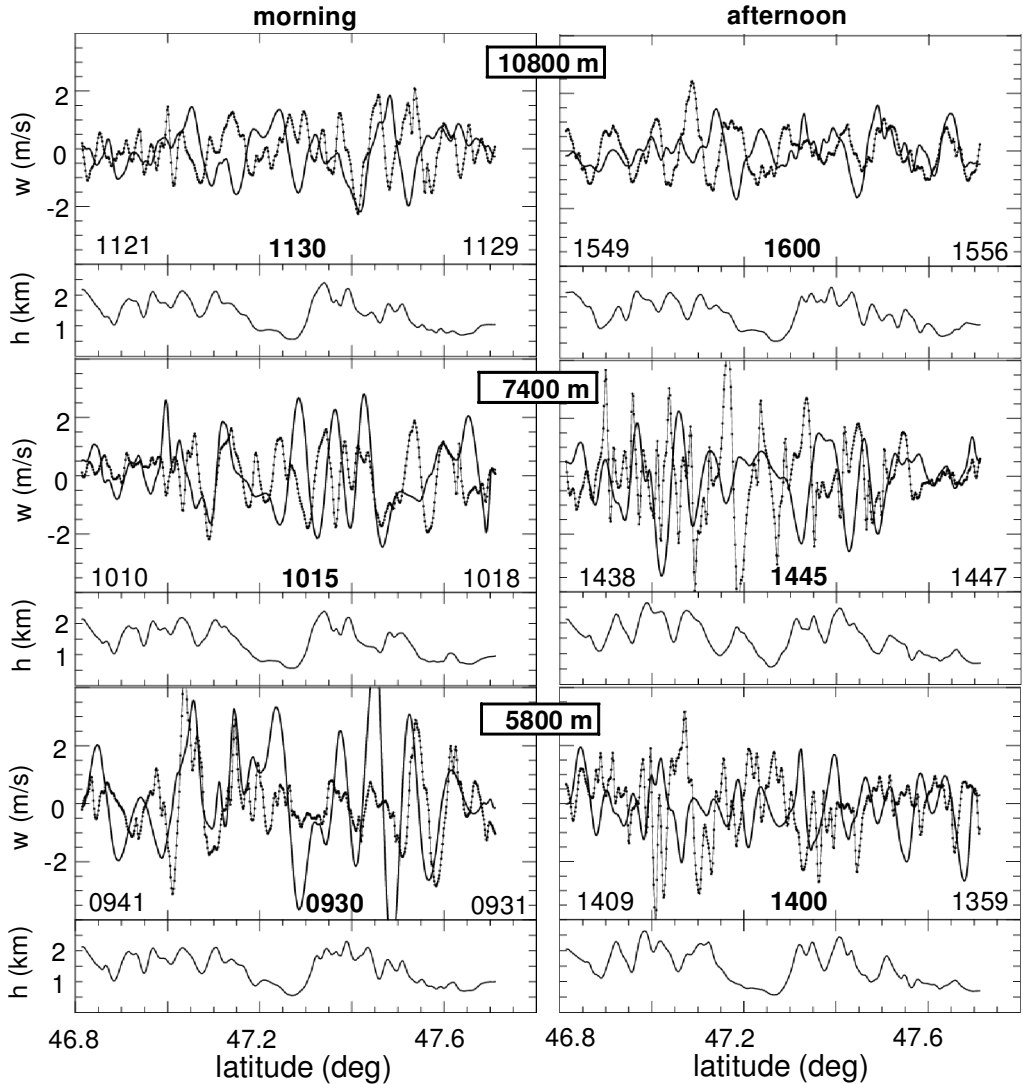


Figure 8. Vertical velocity ( $\text{m s}^{-1}$ ) from the research-aircraft measurements (dotted lines; one value per second) and model simulations along the flight paths. The 5800 m, 7400 m, and 10 800 m altitudes are given for the morning (left) and afternoon (right) flights. The times in each traverse correspond to model output (bold) and aircraft entering and leaving the region (note the changes in direction). The topography (km) is displayed beneath the vertical velocity for each flight leg. The topography varies, as an exact repetitive track was not possible.

generation, amplification and breakdown over complex topography. The results from this particular case illustrate the difficulties of simulating gravity waves in three dimensions over complex topography even with the application of a high-resolution model, in particular for situations such as considered here that feature both vertically propagating and trapped lee waves in the presence of a temporally varying mean state. The predictability of the complex gravity-wave response in this case appears to be limited relative to situations dominated by stationary trapped lee waves such as those described by Shutts and Broad (1993) and Broad (1996). The predictability in this case is also likely to be restricted by initial and lateral boundary-condition errors that can impact the time-dependent evolution of the stability and winds and ultimately the gravity-wave response.

This investigation serves to underscore the importance of repeated research flight legs oriented along the flow over the highest topography to observe non-steady gravity waves adequately, a strategy that

was successfully adopted during the MAP (see, for example, Smith *et al.* 2002). Also, the gravity-wave characteristics observed and simulated in this case highlight the need for dropsondes and remote sensing, such as down-looking lidar onboard the research aircraft, in order to produce a meaningful depiction of the environment and gravity-wave response. Investigations of several MAP cases illustrate the importance of dropsondes to document the upstream vertical structure of the static stability and winds, as well as the upstream and downstream mountain boundary-layer characteristics (Smith *et al.* 2002; Doyle and Smith 2002). Additionally, these studies demonstrate that remote sensing from lidars and rapid-scan satellite imagery can provide valuable depictions of the steadiness of the flow and vertical distribution of the gravity-wave properties. Clearly this pre-MAP investigation would have greatly benefited from these observing systems. Further investigations of the dynamics and predictability of gravity waves observed during the MAP is the topic of a continuing international collaborative research effort. Preliminary results from these ongoing studies of MAP gravity-wave events reveal that the gap between observations and numerical simulation is indeed diminishing.

## ACKNOWLEDGEMENTS

J. D. Doyle was supported by the Office of Naval Research's Program Element 0601153N, with computing time supported in part by a grant of High Performance Computing time from the Department of Defense Shared Resource Center, Stennis Space Center, MS.

## REFERENCES

- Bougeault, P., Binder, P., Buzzi, A., Dirks, R., Houze, R., Kuettner, J., Smith, R. B., Steinacker, R. and Volkert, H. 2001 The MAP Special Observing Period. *Bull. Am. Meteorol. Soc.*, **82**, 433–462
- Bretherton, F. P. 1969 Momentum transport by gravity waves. *Q. J. R. Meteorol. Soc.*, **95**, 213–243
- Broad, A. 1996 High-resolution numerical-model integrations to validate gravity-wave drag parametrization schemes: A case-study. *Q. J. R. Meteorol. Soc.*, **122**, 1625–1653
- Clark, T. L. and Peltier, W. R. 1977 On the evolution and stability of finite amplitude mountain waves. *J. Atmos. Sci.*, **34**, 1715–1730
- Clark, T. L., Hall, W. D., Kerr, R. M., Middleton, D., Radke, L., Ralph, F. M., Neiman, P. J. and Levinson, D. 2000 Origins of aircraft-damaging clear-air turbulence during the 9 December 1992 Colorado downslope windstorm: numerical simulations and comparison with observations. *J. Atmos. Sci.*, **57**, 1105–1131
- Dörnbrack, A. and Dürbeck, T. 1998 Turbulent dispersion of aircraft exhausts in regions of breaking gravity waves. *Atmos. Environ.*, **32**, 3105–3112
- Doyle, J. D. and Smith, R. B. 2002 Mountain waves over the Hohe Tauern. (Submitted to *Q. J. R. Meteorol. Soc.*)
- Doyle, J. D., Durran, D. R., Colle, B. A., Chen, C., Georgelin, M., Grubisic, V., Hsu, W. R., Huang, C. Y., Landau, D., Lin, Y. L., Poulos, G. S., Sun, W. Y., Weber, D. B., Wurtele, M. G. and Xue, M. 2000 An intercomparison of model predicted wave breaking for the 11 January 1972 Boulder windstorm. *Mon. Weather Rev.*, **128**, 901–914
- Durran, D. R. 1990 Mountain waves and downslope winds. *Atmospheric processes over complex topography*. Ed. W. Blumen. American Meteorological Monograph, Vol. 23, **45**, 59–81
- Hodur, R. M. 1997 The Naval Research Laboratory's Coupled Ocean/Atmosphere Mesoscale Prediction System (COAMPS). *Mon. Weather Rev.*, **125**, 1414–1430
- Hoinka, K. P. 1990 Untersuchung der alpinen Gebirgsüberströmung bei Südföhn. DLR Forschungsbericht, DLR-FB 90-30, ISSN 0939-2963. (Available from DLR, Library/Reports, Linder Höhe, D-51147 Köln, Germany.)
- Hoinka, K. P. and Clark, T. L. 1991 Pressure drag and momentum flux due to the Alps. I: Comparison between numerical simulation and observations. *Q. J. R. Meteorol. Soc.*, **117**, 495–525
- Lilly, D. K. 1978 A severe downslope windstorm and aircraft turbulence event induced by a mountain wave. *J. Atmos. Sci.*, **35**, 59–77

- Ralph, F. M., Neiman, P. J., Keller, T. L., Levinson, D. and Fedor, L. 1997 Observations, simulations, and analysis of nonstationary trapped lee waves. *J. Atmos. Sci.*, **54**, 1308–1333
- Satomura, T. and Bougeault, P. 1994 Numerical simulation of lee wave events over the Pyrenees. *J. Meteorol. Soc. Jpn.*, **72**, 173–195
- Schär, C. and Smith, R. B. 1993 Shallow-water flow past isolated topography. Part I: Vorticity production and wake formation. *J. Atmos. Sci.*, **50**, 1373–1400
- Scorer, R. S. 1949 The theory of waves in the lee of mountains. *Q. J. R. Meteorol. Soc.*, **75**, 41–56
- Shutts, G. J. 1998 Stationary gravity-wave structure in flows with directional wind shear. *Q. J. R. Meteorol. Soc.*, **124**, 1421–1442
- Shutts, G. and Broad, A. 1993 A case-study of lee waves over the Lake District in northern England. *Q. J. R. Meteorol. Soc.*, **119**, 377–408
- Smith, R. B. 1979 The influence of mountains on the atmosphere. *Adv. Geophys.*, **21**, 87–230
- Smith, R. B., Skubis, S. T., Doyle, J. D., Broad, A., Kiemle, C. and Volkert, H. 2002 Mountain waves over Mt. Blanc: Influence of a stagnant boundary layer. *J. Atmos. Sci.*, **59**, 2073–2092
- Wurtele, M. G., Sharman, R. D. and Datta, A. 1996 Atmospheric lee waves. *Ann. Rev. Fluid Mech.*, **27**, 429–476